AIAA JOURNAL
Vol. 34, No. 1, January 1996

Matching Inviscid/Boundary-Layer Flowfields

Fred R. DeJarnette* and Robert A. Radcliffe†
North Carolina State University, Raleigh, North Carolina 27695-7910

New boundary-layer equations are developed and the solutions match all of the boundary-layer properties, except for the normal velocity, exactly with the corresponding inviscid properties. The numerical procedure solves tridiagonal matrices at each marching station. As part of the solution an inviscid transpiration velocity at the surface is calculated from the boundary-layer solution. This transpiration velocity could be used as a boundary condition to calculate a new inviscid solution. If the inviscid/boundary-layer solutions are interacted, then the normal velocity from the boundary-layer solution will match the inviscid values exactly. Solutions are calculated for shear flows over a flat plate. Results from the present method compared well with Navier–Stokes solutions for incompressible constant shear flow and sinusoidal shear flow. Iterations of the inviscid/boundary-layer solutions were not necessary. Compressible flow of an exponential shear at Mach 3 was calculated for cold and hot walls. It was found that inviscid/boundary-layer interactions were significant for hot walls but negligible for cold walls. The present method should yield accurate boundary-layer solutions at Reynolds numbers lower than the traditional boundary-layer equations.

Nomenclature

A_j, B_j, C_j, D_j	= coefficients in Eq. (26)
C_f	= skin-friction coefficient, Eq. (29)
F	= u/U_w
F_e	= U/U_w
f	= function defined by Eq. (21) for incompressible flow or by Eq. (41) for compressible flow
f_e	= function defined by Eq. (22) for incompressible flow or by Eq. (42) for compressible flow
g	= H/H_{ew}
H	= $h + u^2/2$
h	= static enthalpy
i, j	= indices for ξ and η grid points
J	= maximum value of j index
L	= reference length
M	= inviscid Mach number
P	= inviscid static pressure
Pr	= Prandtl number
Q_w	= dimensionless heat transfer rate, $q_w\sqrt{(Re_x)}/(\rho_{ew}U_w^3)$
q_w	= heat transfer rate at wall
Re	= Reynolds number, $\rho_{ew}U_wL/\mu_{ew}$
Re_x	= Reynolds number, $\rho_{ew}U_wx/\mu_{ew}$
r	= body radius for axisymmetric flow
T	= temperature
U, V	= inviscid velocity components in x, y directions, respectively
$\bar{V}$	= inviscid normal velocity component given by Eq. (11)
V_w	= transpiration velocity used in inviscid solution
$\bar{V}_w$	= inviscid transpiration velocity calculated from boundary-layer solution
x	= coordinate along body surface
u, v	= boundary-layer velocity components in x, y directions, respectively
y	= coordinate normal to surface
y_e	= value of y at outer boundary
α, β	= parameters in exponential shear flow; see Eq. (59)
γ	= ratio of specific heats
δ	= boundary-layer thickness
δ^*	= displacement thickness
ε	= small parameter to test outer boundary location
η	= transformed coordinate given by Eq. (16) for incompressible or by Eq. (38) for compressible flow
η_e	= value of η at outer boundary
μ	= coefficient of viscosity
ξ	= transformed coordinate given by Eq. (19) for incompressible or by Eq. (37) for compressible flow
ρ	= density
τ_w	= wall shear stress
υ	= kinematic viscosity

Subscripts

e	= inviscid
ew	= inviscid value at wall
w	= wall
∞	= undisturbed freestream

Superscript

$*$	= value at displacement surface

Introduction

WHEN finite difference boundary-layer codes are coupled with inviscid flowfield codes, the matching of the two flowfields poses a problem. This is particularly true for inviscid shear and entropy layers near the edge of the boundary layer. Classical boundary-layer methods neglect these layers. Even when they are considered, most boundary-layer methods assume the flowfield properties approach the inviscid values at the boundary-layer edge with a zero slope. This assumption is particularly poor for lower Reynolds numbers where the boundary-layer thickness is a significant fraction of the shock layer, and it is one of the reasons some investigators jumped from using boundary-layer methods to fully viscous shock layers. If the boundary-layer solution does not match the inviscid solution well, then surface properties such as skin-friction and heat transfer rates are not calculated accurately. This

Presented as Paper 94-0128 at the AIAA 32nd Aerospace Sciences Meeting, Reno, NV, Jan. 10–13, 1994; received Aug. 18, 1994; revision received May 30, 1995; accepted for publication July 5, 1995.

*Head, Mechanical and Aerospace Engineering, Box 7910. Associate Fellow AIAA.

†Graduate Research Assistant, Aerospace Engineering, Box 7910. Student Member AIAA.

paper develops a new method for matching inviscid-boundary-layer flowfields.

The traditional method of calculating the boundary-layer properties is to first calculate an inviscid flowfield neglecting the boundary layer. Then the inviscid properties on the body surface are used as edge conditions for the boundary-layer solution. However, when a shear layer exists near the surface in the inviscid solution, the inviscid properties (other than pressure) at the edge of the boundary layer can be significantly different from those on the surface. For these flowfields the boundary-layer solution will yield more accurate results if the inviscid properties at a distance δ from the surface are used as edge conditions. This procedure was employed in Ref. 1 using the HALIS inviscid code and the approximate heating relations of Zoby et al.[2] A similar procedure was used by Riley and DeJarnette[3] that combined an approximate inviscid code with the approximate heating relations[2] to calculate heating rates.[4]

The technique just described works well for Reynolds numbers high enough that the boundary-layer thickness remains small compared with the shock-layer thickness. However, at the lower Reynolds numbers where the boundary layer occupies a significant part of the shock layer, interactive inviscid/boundary-layer or viscous shock-layer methods are needed. It was found recently[5] that interactive inviscid/boundary-layer results compare well with viscous shock-layer results for a blunted 5-deg cone at a Mach number of 15 and 150,000-ft altitude. Under these conditions the interactive effects are significant for the surface pressure as well as the heat transfer rates.

Numerous authors have developed coupled Euler/boundary-layer methods.[6–8] They generally use the second-order boundary-layer equations and some form of Van Dyke's matched asymptotic expansions. Iterations are required between the Euler and boundary-layer solutions. The matching of the two regions generally has problems when the inviscid flow has significant normal gradients. Aupoix et al.[6] removed many of these deficiencies by developing an asymptotic defect method. However, they require a first-order defect solution, a new Euler solution, and then a second-order defect solution. The boundary-layer equations used are first order and second order, respectively. The solution procedure is somewhat awkward in that two different sets of equations must be solved. Also, some of the incompressible shear flows compared poorly with the Navier–Stokes results.

The method presented here uses a new form of the boundary-layer equations that matches exactly all of the properties except the normal velocity component. By interacting the inviscid and boundary-layer solutions the normal velocity can also be matched.

Analysis

To understand the basic approach used here, we will consider first the special case of steady, two-dimensional, incompressible, laminar flow. Once the matching technique for this special case is verified, the more general case of compressible flow can be considered. The inviscid equations that are solved for this special case are

Continuity:

$$\frac{\partial U}{\partial x}+\frac{\partial V}{\partial y}=0 \tag{1}$$

x momentum:

$$U\frac{\partial U}{\partial x}+V\frac{\partial U}{\partial y}=-\frac{1}{\rho}\frac{\partial P}{\partial x} \tag{2}$$

y momentum:

$$U\frac{\partial V}{\partial x}+V\frac{\partial V}{\partial y}=-\frac{1}{\rho}\frac{\partial P}{\partial y} \tag{3}$$

subject to the boundary conditions at

$$y=0, \qquad V(x,0)=0 \tag{4}$$

as

$$y\to\infty, \qquad U^2+V^2=U_\infty^2+V_\infty^2 \tag{5}$$

After obtaining the inviscid solution, the traditional first-order boundary-layer solution uses only $U(x,0)$ from the inviscid solution. The first-order, laminar boundary-layer equations are as follows:

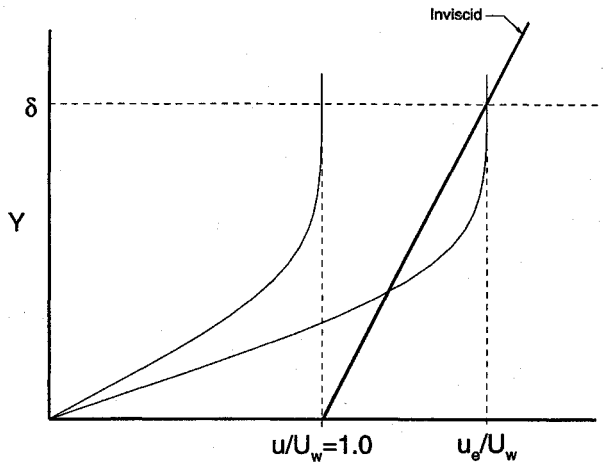

Fig. 1 Velocity profiles for other methods.

Continuity:

$$\frac{\partial u}{\partial x}+\frac{\partial v}{\partial y}=0 \tag{6}$$

x momentum:

$$u\frac{\partial u}{\partial x}+v\frac{\partial u}{\partial y}-\upsilon\frac{\partial^2 u}{\partial y^2}=-\frac{1}{\rho}\frac{\partial P}{\partial x} \tag{7}$$

The y-momentum equation is simply $(\partial P/\partial y)=0$, which makes $P=P(x)$. Traditional boundary-layer theory applies Eq. (2) at the wall to obtain

$$U\frac{\mathrm{d}U}{\mathrm{d}x}=-\frac{1}{\rho}\frac{\mathrm{d}P}{\mathrm{d}x}$$

Using this result for the right-hand side, Eq. (7) is rewritten as

$$u\frac{\partial u}{\partial x}+v\frac{\partial u}{\partial y}-\upsilon\frac{\partial^2 u}{\partial y^2}=U\frac{\mathrm{d}U}{\mathrm{d}x} \tag{7a}$$

The boundary conditions are at

$$y=0, \qquad u(x,0)=0 \quad \text{and} \quad v(x,0)=0 \tag{8}$$

as

$$y\to\infty, \qquad u=U(x,0) \tag{9}$$

It is assumed that $U=U(x,0)$ across the boundary layer in the preceding equations. For $y\to\infty$ only the first term on the left-hand side of Eq. (7) has an equivalent inviscid term on the right-hand side. Consequently, the second and third terms on the left-hand side must approach zero, which forces

$$\frac{\partial u}{\partial y}\to 0 \quad \text{and} \quad \frac{\partial^2 u}{\partial y^2}\to 0 \quad \text{as} \quad y\to\infty$$

A typical velocity profile for Eqs. (6–9) is illustrated in Fig. 1. Note that if U varies with y, then u does not match U in magnitude or slope at the outer boundary. Also, the vertical velocity component v does not match V in the inviscid solution. Some boundary-layer methods replace Eq. (9) with $u=U(x,\delta)$ at $y=\delta$. Although this technique matches u to $U(x,\delta)$ at $y=\delta$, Fig. 1 shows that the slope is not matched there. In addition, it is difficult to define δ precisely.

The proper matching of the boundary-layer solution with the inviscid solution would have

$$u=U(x,y) \quad \text{and} \quad v=V(x,y) \quad \text{for} \quad y\geq\delta \tag{10}$$

and it is illustrated in Fig. 2. The boundary conditions given by Eq. (10) will match the boundary-layer flowfield with the inviscid flowfield exactly. However, since $(\partial v/\partial y)$ is the highest y derivative on v, there can be only one boundary condition imposed on v, and

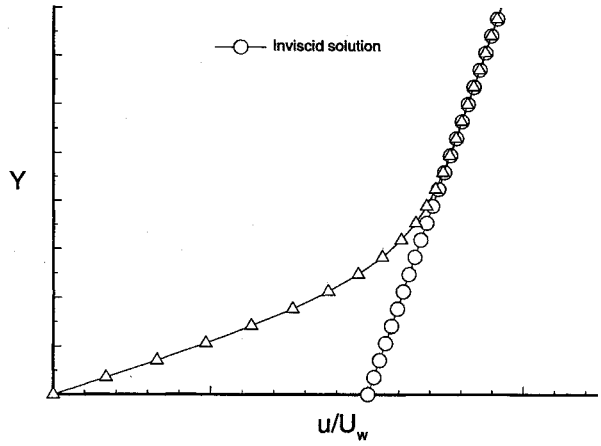

Fig. 2 Velocity profiles for new method.

the no-slip condition given in Eq. (8) has already been used. On the other hand the outer boundary condition on v given by Eq. (10) can be used if an additional unknown in the boundary-layer solution is introduced. Here that unknown is $\bar{V}_w(x)$, which is the inviscid transpiration velocity at the wall. It is well known that the inviscid flowfield must be displaced a distance δ^* from the actual body surface to account for the mass defect in the boundary layer. This effect can also be accomplished by giving the inviscid flowfield a transpiration velocity $V_w(x)$ to displace the outer flow from the surface. Thus $V(x, 0) = V_w(x)$ replaces Eq. (4) as a boundary condition for the inviscid solution. Unless the boundary layer and inviscid solutions are interacted, $\bar{V}_w$ calculated in the boundary-layer solution is not the same as $V_w(x)$ used in the inviscid solution.

For the new matching method developed here, only $U(x, y)$ is used from the inviscid solution. Equation (1) is integrated to give

$$\bar{V} = \bar{V}_w(x) - \int_0^y \frac{\partial U}{\partial x} dy \tag{11}$$

This vertical velocity will differ from the actual $V(x, y)$ unless $\bar{V}_w(x)$ from the boundary-layer solution is the same as $V_w(x)$ used as a boundary condition in the inviscid solution. If the boundary-layer solution is interacted with the inviscid solution, then $\bar{V}_w(x)$ from the boundary-layer solution could be used as $V_w(x)$ to calculate a new inviscid solution. A converged solution would produce $\bar{V}_w(x) = V_w(x)$ and hence $\bar{V} = V$.

As a first attempt to match $u(x, y)$ with $U(x, y)$, Eq. (2) is used to replace the right-hand side of Eq. (7), which gives

$$u\frac{\partial u}{\partial x} + v\frac{\partial u}{\partial y} - \upsilon\frac{\partial^2 u}{\partial y^2} = U\frac{\partial U}{\partial x} + V\frac{\partial U}{\partial y} \tag{7b}$$

This equation is an improvement over Eq. (7a) because the first and second terms on the left-hand side have corresponding inviscid terms on the right-hand side. However, even with V replaced by $\bar{V}$, exact matching of $u(x, y)$ with $U(x, y)$ will occur only if $\upsilon(\partial^2 U/\partial y^2) = 0$ at the outer boundary. Although the inviscid flowfield equations, Eqs. (1–3), do not contain viscous terms, it is generally found that $\upsilon(\partial^2 U/\partial y^2)$ is not zero. However, for the computed inviscid flowfield to be accurate outside the boundary layer, the magnitude of this term must be small in comparison with the other terms in Eq. (2). This is one of the terms that is neglected in the Navier–Stokes equations to obtain Euler's equations. Therefore, this term is added to the right-hand side of Eq. (7b) along with replacing V with $\bar{V}$ to obtain the new boundary-layer equation

$$u\frac{\partial u}{\partial x} + v\frac{\partial u}{\partial y} - \upsilon\frac{\partial^2 u}{\partial y^2} = U\frac{\partial U}{\partial x} + \bar{V}\frac{\partial U}{\partial y} - \upsilon\frac{\partial^2 U}{\partial y^2} \tag{12}$$

Also, the outer boundary condition given by Eq. (9) is replaced by

$$u = U(x, y_e) \quad \text{and} \quad v = \bar{V}(x, y_e) \quad \text{for} \quad y = y_e \geq \delta \tag{13}$$

Now each inviscid term on the right-hand side of Eq. (12) matches a corresponding term on the left-hand side. If y_e is sufficiently large, there will be an exact matching of u with $U(x, y)$ and v with $\bar{V}(x, y)$. The inclusion of the additional terms on the right-hand side of Eq. (12) forces u to match the variation of U with y, although no boundary condition on $(\partial u/\partial y)$ is imposed at the outer boundary. The boundary condition $v = \bar{V}$ at $y = y_e$ in Eq. (13) determines $\bar{V}_w(x)$, and therefore some of the boundary layer/inviscid interaction is included in the initial boundary-layer calculations. If $U(x, y) = U(x, 0)$, then Eq. (12) reduces to the traditional first-order boundary-layer equation given by Eq. (7a). Properly matching the boundary-layer solution with the inviscid solution increases the accuracy of the skin friction also, as will be shown next.

Determination of $\bar{V}_w(x)$

Integrate Eq. (6) to obtain

$$v(x, y) = -\int_0^y \frac{\partial u}{\partial x} dy \tag{14}$$

For $y \geq \delta$, Eqs. (11), (13), and (14) combine to give

$$\bar{V}_w(x) - \int_0^\delta \frac{\partial U}{\partial x} dy = -\int_0^\delta \frac{\partial u}{\partial x} dy$$

which can be rewritten as

$$\bar{V}_w(x) = \frac{d}{dx}\int_0^\delta (U - u) dy \tag{15}$$

Equation (15) gives the transpiration velocity $\bar{V}_w(x)$ for the inviscid solution. The precise definition of δ is not required because the integrand of the integral in Eq. (15) goes to zero for $y \geq \delta$.

Shear Flow over a Flat Plate

The method outlined earlier is applied to shear flow over a flat plate. The inviscid shear flows considered here have $U(x, y) = U(y)$.

Define Blasius parameters

$$\eta = y\sqrt{\frac{U_w}{x\upsilon}} \tag{16}$$

and

$$\frac{u}{U_w} = \frac{\partial f}{\partial \eta} \equiv F(\xi, \eta) \tag{17}$$

Also, define

$$\frac{U}{U_w} = \frac{\partial f_e}{\partial \eta} \equiv F_e(\xi, \eta) \tag{18}$$

where U_w is the inviscid velocity at $y = 0$, which is constant here. Since Eq. (16) gives $y = \eta\sqrt{(x\upsilon/U_w)}$, it is necessary to define

$$\xi = \sqrt{x/L} \tag{19}$$

This definition makes $(y\sqrt{Re/L}) = \xi\eta$ and $(\partial Fe/\partial\xi)$ finite at $x = 0$. (Note that if we had defined $\xi = x/L$ and consider linear shear flow, i.e., $Fe = 1 + \omega y/L$, then $\partial Fe/\partial\xi = \infty$ at $x = 0$.) With ξ and η as independent variables, substitute Eqs. (16–19) into Eqs. (11), (12), and (14) to obtain

$$\frac{f}{2}\frac{\partial F}{\partial \eta} - \frac{\xi}{2}\left[F\frac{\partial F}{\partial \xi} - \frac{\partial f}{\partial \xi}\frac{\partial F}{\partial \eta}\right] + \frac{\partial^2 F}{\partial \eta^2}$$
$$= \frac{f_e}{2}\frac{\partial F_e}{\partial \eta} - \frac{\xi}{2}\left[F_e\frac{\partial F_e}{\partial \xi} - \frac{\partial f_e}{\partial \xi}\frac{\partial F_e}{\partial \eta}\right] + \frac{\partial^2 F_e}{\partial \eta^2} \tag{20}$$

and Eqs. (17) and (18) integrate to

$$f = \int_0^\eta F\, d\eta \tag{21}$$

$$f_e = f_{ew}(\xi) + \int_0^\eta F_e d\eta \tag{22}$$

The term $f_{ew}(\xi)$ is the mass flux at the wall in the inviscid flow to account for the boundary-layer mass defect, and it is generally negative. The boundary conditions are at

$$\eta = 0, \qquad f(\xi, 0) = 0, \qquad F(\xi, 0) = 0 \tag{23}$$

at

$$\eta = \eta_e, \qquad f = f_e \qquad \text{and} \qquad F = F_e \tag{24}$$

The inviscid solution gives $F_e(\xi, \eta)$. The boundary-layer solution yields $f_{ew}(\xi)$ from Eqs. (21), (22), and (24) as

$$f_{ew} = \int_0^{\eta_e} (F - F_e)\, d\eta \tag{24a}$$

It is related to $\bar{V}_w(\xi)$, by using Eqs. (21), (22), and (24) to rewrite Eq. (15) as

$$\frac{\bar{V}_w \sqrt{Re_x}}{U_w} = -\frac{1}{2}\frac{d}{d\xi}(\xi f_{ew}) \tag{25}$$

Thus, $f = f_e$ at $\eta = \eta_e$ in Eq. (24) is equivalent to satisfying Eq. (13) as the new boundary condition.

Solution Procedure

The partial differential equation given by Eq. (20) is discretized by using a fully implicit finite difference method for the η direction and a two-point backward difference quotient for the ξ derivatives.[9,10] This finite difference method was chosen because it is easy to implement, fast, reasonably accurate, and unconditionally stable.[10] However, any other finite difference method for boundary layers could have been used. With $\xi_i = \xi_{i-1} + \Delta\xi$ and $\eta_j = \eta_{j-1} + \Delta\eta$, the partial derivatives in Eq. (20) are replaced by the following difference quotients for a uniform grid spacing:

$$\frac{\partial F}{\partial \xi} = \frac{F_{i,j} - F_{i-1,j}}{\Delta\xi}$$

$$\frac{\partial F}{\partial \eta} = \frac{F_{i,j+1} - F_{i,j-1}}{2\Delta\eta}$$

$$\frac{\partial^2 F}{\partial \eta^2} = \frac{F_{i,j+1} - 2F_{i,j} + F_{i,j-1}}{\Delta\eta^2}$$

The equation $(\partial f/\partial \eta) = F$ is discretized as

$$\frac{f_{i,j} - f_{i,j-1}}{\Delta\eta} = \frac{1}{2}(F_{i,j} + F_{i,j-1})$$

The same finite difference quotients are used for the inviscid terms on the right-hand side of Eq. (20). Using the finite difference replacements, Eq. (20) can be locally linearized[9] and written in tridiagonal matrix form[10] as

$$-A_j F_{j-1} + B_j F_j - C_j F_{j+1} = D_j \tag{26}$$

for $j = 2, \ldots, J-1$. The boundary conditions are at

$$\eta = 0\,(j = 1), \qquad F_1 = 0, \qquad f_1 = 0, \qquad f_{e_1} = f_{ew} \tag{27}$$

at

$$\eta = \eta_e\,(j = J), \qquad F_J = F_{e_J}, \qquad f_J = f_{e_J} \tag{28}$$

Equation (26) is solved iteratively by the scalar Thomas algorithm.[9] In the first iteration at each marching station, the coefficients in Eq. (26) and f_{ew} are evaluated at the previous marching station. In successive iterations these coefficients are recomputed with quantities from the previous iteration. The value of f_{ew} is updated at the end of each iteration by Eq. (24a).

The solution starts at $\xi = 0$ where Eq. (20) reduces to an ordinary differential equation that can be solved by Eqs. (26–28). Then the solution can be "marched" to the next $\xi_i = \xi_{i-1} + \Delta\xi$ station by solving the same system of equations but with new coefficients. In this procedure it is only necessary to save the solution at the previous ξ station. The solution can be marched from $\xi = 0$ to the end of the body or to the separation point, whichever comes first.

The value chosen for η_e does not need to be precise as long as $F_j = F_{e_j} - \varepsilon$ at $j = J-1$ and $J-2$, and ε can be made as small as you please, consistent with the precision of the computer used. For single precision, a typical value is $\varepsilon = 10^{-5}$. If η_e is too small, then simply make η_e larger until this criterion is met. When η_e is larger than necessary, then $F_j = F_{e_j} - \varepsilon$ for some $j < J-2$.

Boundary-Layer Parameters

The transpiration velocity, $(\bar{V}_w/U_w)\sqrt{(Re_x)}$, can be calculated from Eq. (25). The skin-friction coefficient is given by

$$C_f = \frac{2\tau_w}{\rho U_w^2}, \qquad \text{where} \qquad \tau_w = \mu\left(\frac{\partial u}{\partial y}\right)_w \tag{29}$$

Substitute Eqs. (16) and (17) into Eq. (29) to get

$$C_f\sqrt{Re_x} = 2\left(\frac{\partial F}{\partial \eta}\right)_w \tag{30}$$

The displacement thickness δ^* is the value of y where $f_e = 0$. The corresponding value of $\eta = \eta^*$ is determined by interpolation of the $(f_e)_j$ data to determine where $f_e = 0$. Then using Eq. (16),

$$(\delta^*/x)\sqrt{Re_x} = \eta^* \tag{31}$$

Compressible Boundary Layers

The traditional equations governing the compressible, laminar boundary layer for two-dimensional or axisymmetric flow are[10]

Continuity:

$$\frac{\partial(\rho u r)}{\partial x} + \frac{\partial(\rho v r)}{\partial y} = 0 \tag{32}$$

x momentum:

$$\rho u\frac{\partial u}{\partial x} + \rho v\frac{\partial u}{\partial y} - \frac{\partial}{\partial y}\left(\mu\frac{\partial u}{\partial y}\right) = -\frac{\partial P}{\partial x} \tag{33}$$

The same justification as used for Eq. (12) is used to rewrite the right-hand side of Eq. (33) as

$$-\frac{\partial P}{\partial x} \approx \rho_e U\frac{\partial U}{\partial x} + \rho_e \bar{V}\frac{\partial U}{\partial y} - \frac{\partial}{\partial y}\left(\mu_e\frac{\partial U}{\partial y}\right) \tag{33a}$$

Thus the new momentum equation has the right-hand side of Eq. (33a) for $-\partial P/\partial x$ in Eq. (33) and the same boundary conditions as Eq. (13). The traditional energy equation is

$$\rho u\frac{\partial H}{\partial x} + \rho v\frac{\partial H}{\partial y} - \frac{\partial}{\partial y}\left(\frac{\mu}{Pr}\frac{\partial H}{\partial y}\right) - \left(1 - \frac{1}{Pr}\right)\frac{\partial}{\partial y}\left(\mu u\frac{\partial u}{\partial y}\right) = 0 \tag{34}$$

where $H = h + u^2/2$ and $r(x)$ is the body radius for axisymmetric flow and $r = 1$ for two-dimensional flow. Note that H is not exactly the total enthalpy since v is not included in it. It is, however, approximately equal to the total enthalpy. In the inviscid solution, the total enthalpy, $h_e + (U^2 + V^2)/2$, is constant and $H_e = h_e + U^2/2$ is nearly constant. Hence

$$\rho_e U\frac{\partial H_e}{\partial x} + \rho_e V\frac{\partial H_e}{\partial y} \approx 0 \tag{34a}$$

In the traditional boundary-layer solution, Eq. (34) forces $(\partial H/\partial y) \to 0$ and $(\partial^2 H/\partial y^2) \to 0$ as $y \to \infty$. This does not, in general, match H with H_e unless H_e is constant. To match H with H_e exactly, it is necessary to add inviscid terms on the right-hand

side (RHS) of Eq. (34) that correspond to the terms on the left-hand side, i.e.,

$$\text{RHS} = \rho_e U \frac{\partial H_e}{\partial x} + \rho_e \bar{V} \frac{\partial H_e}{\partial y} - \frac{\partial}{\partial y}\left(\frac{\mu_e}{Pr}\frac{\partial H_e}{\partial y}\right)$$
$$-\left(1 - \frac{1}{Pr}\right)\frac{\partial}{\partial y}\left(\mu_e U \frac{\partial U}{\partial y}\right) \tag{34b}$$

The last two terms in the preceding equation are heat transfer and shear work, which were neglected in the inviscid energy equation. As with the x-momentum equation, the magnitude of these terms must be small in comparison with the others for the calculated inviscid flowfield to be accurate outside the boundary layer. The new energy equation is Eq. (34) except the right-hand side is given by Eq. (34b). The solution to the inviscid flowfield supplies U, P, and H_e. The inviscid vertical velocity $\bar{V}$ is obtained from integrating Eq. (32) and it involves $\bar{V}_w$, which is determined from the boundary-layer solution. The boundary conditions for Eqs. (32–34b) are at

$$y = 0; \qquad u = 0, \qquad v = 0, \tag{35}$$

and either $H_w(x)$ or an adiabatic wall is specified. For

$$y = y_e \geq \delta; \qquad u = U(x, y_e)$$
$$v(x, y) = \bar{V}(x, y_e) \qquad \text{and} \qquad H = H_e(x, y_e) \tag{36}$$

Generally a transformation of coordinates is needed to remove the singularity at $x = 0$, reduce the growth of the boundary layer in the transformed coordinates, and incorporate the Mangler transformation for axisymmetric flows. Most transformations for compressible flows employ the Levy–Lees transformation,[10] which involves inviscid properties at the edge of the boundary layer. For the matching procedure used here, the edge of the boundary layer is not known a priori, and in addition, it is difficult to define precisely. Therefore, the inviscid properties used in the present transformation are those on the surface, i.e., ρ_{ew}, U_w, H_{ew}, etc. The new transformation thus becomes

$$\xi(x) = \int_0^x (\rho_e \mu_e U)_w r^2 \mathrm{d}x \tag{37}$$

$$\eta(x, y) = \frac{\rho_{ew} U_w r}{\sqrt{2\xi}} \int_0^y \frac{\rho}{\rho_{ew}} \mathrm{d}y \tag{38}$$

Define

$$u/U_w = F(\xi, \eta) \tag{39}$$

$$U/U_w = F_e(\xi, \eta) \tag{40}$$

$$f = \int_0^\eta F \mathrm{d}\eta \tag{41}$$

$$f_e = \int_0^\eta \frac{\rho_e F_e}{\rho} \mathrm{d}\eta + f_{ew} \tag{42}$$

Equations (41) and (42) define transformed stream functions for the boundary layer and inviscid flowfields, respectively.

With these transformations and definitions, the x-momentum equation, Eqs. (33) and (33a), becomes

$$2\xi\left[F\left(\frac{F}{U_w}\frac{\mathrm{d}U_w}{\mathrm{d}\xi} + \frac{\partial F}{\partial \xi}\right) - \frac{\partial f}{\partial \xi}\frac{\partial F}{\partial \eta}\right]$$
$$- f\frac{\partial F}{\partial \eta} - \frac{\partial}{\partial \eta}\left(\frac{\rho\mu}{\rho_{ew}\mu_{ew}}\frac{\partial F}{\partial \eta}\right)$$
$$= 2\xi\left[\frac{\rho_e}{\rho}F_e\left(\frac{F_e}{U_w}\frac{\mathrm{d}U_w}{\mathrm{d}\xi} + \frac{\partial F_e}{\partial \xi}\right) - \frac{\partial f_e}{\partial \xi}\frac{\partial F_e}{\partial \eta}\right]$$
$$- f_e\frac{\partial F_e}{\partial \eta} - \frac{\partial}{\partial \eta}\left(\frac{\rho\mu_e}{\rho_{ew}\mu_{ew}}\frac{\partial F_e}{\partial \eta}\right) \tag{43}$$

Define

$$g(\xi, \eta) = H/H_{ew} \tag{44}$$

Then the energy equation, Eqs. (34) and (34b), transforms to

$$2\xi\left[F\left(\frac{g}{H_{ew}}\frac{\mathrm{d}H_{ew}}{\mathrm{d}\xi} + \frac{\partial g}{\partial \xi}\right) - \frac{\partial f}{\partial \xi}\frac{\partial g}{\partial \eta}\right]$$
$$- f\frac{\partial g}{\partial \eta} - \frac{\partial}{Pr\,\partial \eta}\left(\frac{\rho\mu}{\rho_{ew}\mu_{ew}}\frac{\partial g}{\partial \eta}\right)$$
$$-\left(1 - \frac{1}{Pr}\right)\frac{U_w^2}{H_{ew}}\frac{\partial}{\partial \eta}\left(\frac{\rho\mu}{\rho_{ew}\mu_{ew}}F\frac{\partial F}{\partial \eta}\right)$$
$$= 2\xi\left[\frac{\rho_e F_e}{\rho}\left(\frac{g_e}{H_{ew}}\frac{\mathrm{d}H_{ew}}{\mathrm{d}\xi} + \frac{\partial g_e}{\partial \xi}\right) - \frac{\partial f_e}{\partial \xi}\frac{\partial g_e}{\partial \eta}\right]$$
$$- f_e\frac{\partial g_e}{\partial \eta} - \frac{1}{Pr}\frac{\partial}{\partial \eta}\left(\frac{\rho\mu_e}{\rho_{ew}\mu_{ew}}\frac{\partial g_e}{\partial \eta}\right)$$
$$-\left(1 - \frac{1}{Pr}\right)\frac{U_w^2}{H_{ew}}\frac{\partial}{\partial \eta}\left(\frac{\rho\mu_e}{\rho_{ew}\mu_{ew}}F_e\frac{\partial F_e}{\partial \eta}\right) \tag{45}$$

The boundary conditions on Eqs. (44) and (45) are at

$$\eta = 0, \quad F = 0, \quad f = 0, \quad g = g_w, \quad \text{or} \quad \frac{\partial g}{\partial \eta} = 0 \tag{46}$$

at

$$\eta = \eta_e, \qquad F = F_e, \qquad g = g_e, \qquad \text{and} \qquad f = f_e \tag{47}$$

The requirement that $f = f_e$ at $\eta = \eta_e$ is used to determine f_{ew} from Eqs. (41) and (42). Then f_{ew} can be used to calculate $\bar{V}_w$.

Equations (41–43) and (45) are discretized using the same difference scheme as used earlier. The resulting difference equations are linearized[10] and cast in the form of a tridiagonal matrix similar to Eqs. (26–28). They are solved by the Thomas algorithm to obtain F and g across the boundary layer at each ξ station. The Sutherland law is used to calculate the coefficient of viscosity and $Pr = 0.72$ for air.

Compressible Shear Flow over a Flat Plate

Similar to the incompressible shear flow, the inviscid shear flows considered here have $U(x, y) = U(y)$ with $U(y)$ a linear or exponential function of y. In addition to constant pressure, the enthalpy $H_e = h_e + U^2/2$ is constant throughout the inviscid flowfield. We define the inviscid Mach number as the Mach number of the inviscid flow at $y = 0$, i.e.,

$$M_w^2 = \frac{U_w^2}{(\gamma - 1)h_{ew}} \tag{48}$$

The inviscid temperature T_e ratioed to the inviscid temperature at the wall T_{ew} is obtained from the equation for H_e being constant, i.e.,

$$h_e + (U^2/2) = h_{ew} + \left(U_w^2/2\right) \tag{49}$$

For a perfect gas we get

$$(T_e/T_{ew}) = 1 + [(\gamma - 1)/2]M_w^2\left[1 - \left(U^2/U_w^2\right)\right] \tag{50}$$

and

$$\frac{U_w^2}{H_{ew}} = \frac{(\gamma - 1)M_w^2}{1 + [(\gamma - 1)/2]M_w^2}$$

Since the inviscid wall properties are constant, Eqs. (37) and (38) reduce to

$$\xi = \rho_{ew}\mu_{ew}U_w x \tag{51}$$

and

$$\eta = \sqrt{\frac{\rho_{ew}U_w}{2\mu_{ew}x}} \int_0^y \frac{\rho}{\rho_{ew}} \mathrm{d}y \tag{52}$$

The skin-friction coefficient becomes

$$C_f\sqrt{Re_x} = \sqrt{2}\frac{\rho_w}{\rho_{ew}}\frac{\mu_w}{\mu_{ew}}\left(\frac{\partial F}{\partial \eta}\right)_w \tag{53}$$

and

$$Q_w = \frac{q_w\sqrt{Re_x}}{\rho_{ew}U_w^3} = \frac{H_{ew}}{\sqrt{2}PrU_w^2}\frac{\rho_w\mu_w}{\rho_{ew}\mu_{ew}}\left(\frac{\partial g}{\partial \eta}\right)_w$$

For the shear flow used here it is necessary to replace ξ derivatives, with the aid of Eq. (51), with

$$\xi\frac{\partial}{\partial \xi} = \frac{\sqrt{x/L}}{2}\frac{\partial}{\partial(\sqrt{x/L})} \tag{54}$$

Now the marching variable becomes $\sqrt{x/L}$ and $\partial F_e/\partial\sqrt{x/L}$ is finite at $x = 0$. The transpiration velocity $\bar{V}_w$ is obtained in a fashion similar to Eq. (25) as

$$\frac{\bar{V}_w}{U_w}\sqrt{Re_x} = -\frac{1}{\sqrt{2}}\frac{\mathrm{d}}{\mathrm{d}\sqrt{x/L}}(\sqrt{x/L}f_{ew}) \tag{55}$$

The displacement thickness δ^* is obtained from Eq. (52) as

$$\frac{\delta^*}{x}\sqrt{Re_x} = \sqrt{2}\int_0^{\eta^*}\frac{\rho_{ew}}{\rho}\mathrm{d}\eta \tag{56}$$

where η^* is determined by interpolating the numerical solution to find the value of η where $f_e(\xi, \eta^*) = 0$.

Results and Discussion

This paper presents a new method for matching boundary/inviscid flowfields. To illustrate the method, results are presented for nonuniform inviscid flow, which includes shear and entropy layers, over a semi-infinite flat plate. The standard for assessing the accuracy of the results is the solution to the Navier–Stokes equations. The first and simplest case is that of incompressible, inviscid constant shear flow with $Re = 10^6$ given by the equation

$$U/U_w = 1 + 60(y/L) \tag{57}$$

Results for the velocity profile at $x/L = 0.9$ are presented in Fig. 3 and compared with the Navier–Stokes and second-order defect results.[6] Results for the skin-friction variation along the plate are given in Fig. 4. These two figures show that the present method compares very well with both the Navier–Stokes and second-order defect methods. However, the second-order defect method required an iteration on both the inviscid and boundary-layer solutions, whereas the present method did not iterate either solution. Figure 4 illustrates a significant increase in the skin-friction coefficient along the flat plate. The traditional first-order boundary-layer method, Eqs. (6–9), gives a constant value of 0.332 that is the same as the present result at the leading edge.

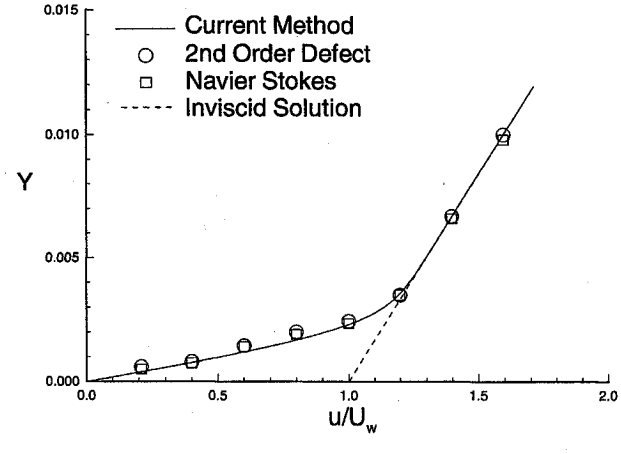

Fig. 3 Velocity profiles for constant shear flow at $x/L = 0.9$.

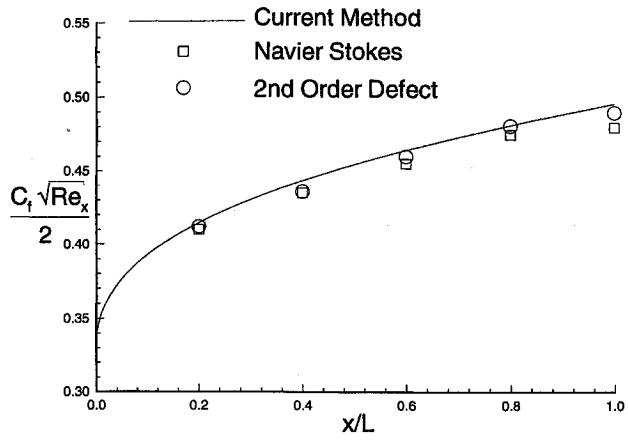

Fig. 4 Skin-friction coefficient for constant shear flow.

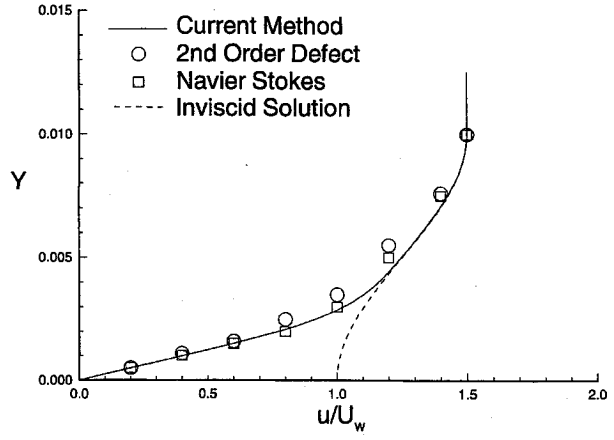

Fig. 5 Velocity profiles for sinusoidal shear flow at $x/L = 0.9$.

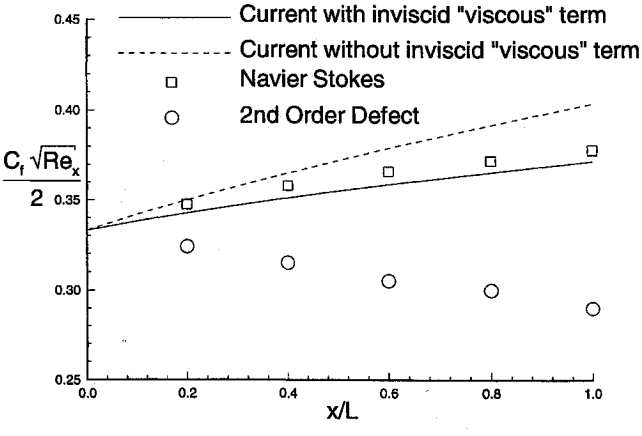

Fig. 6 Skin-friction coefficient for sinusoidal shear flow.

The second case is incompressible inviscid flow with $Re = 10^6$ given by the sinusoidal velocity profile

$$U/U_w = 1 + 0.5\sin^2[50\pi(y/L)] \quad \text{for} \quad y/L < 0.01$$
$$U/U_w = 1.5 \quad \text{for} \quad y/L \geq 0.01 \tag{58}$$

Figure 5 shows the velocity profile at $x/L = 0.9$, and again the present method compares very well with the Navier–Stokes and second-order defect methods.[6] Aupoix et al.[6] called this case the limit of the boundary-layer approach because their second-order defect method failed to reproduce the Navier–Stokes skin-friction solution shown in Fig. 6. However, Fig. 6 shows that the present method predicts skin friction within 2% of the Navier–Stokes results. It also shows that omitting the inviscid viscous term, i.e., $\upsilon(\partial^2 U/\partial y^2)$, decreases the accuracy of the present method. Again, the present method did not iterate the inviscid and

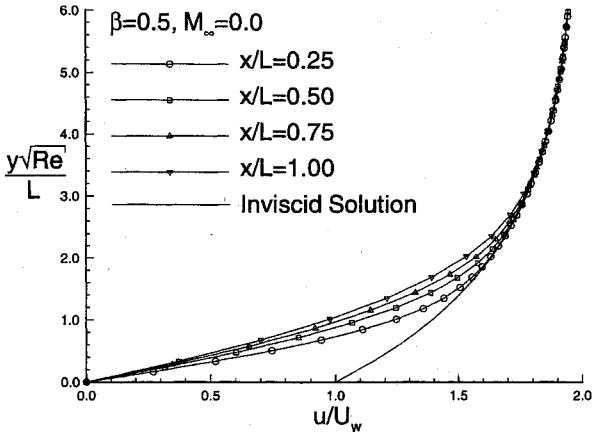

Fig. 7 Velocity profiles for exponential shear flow.

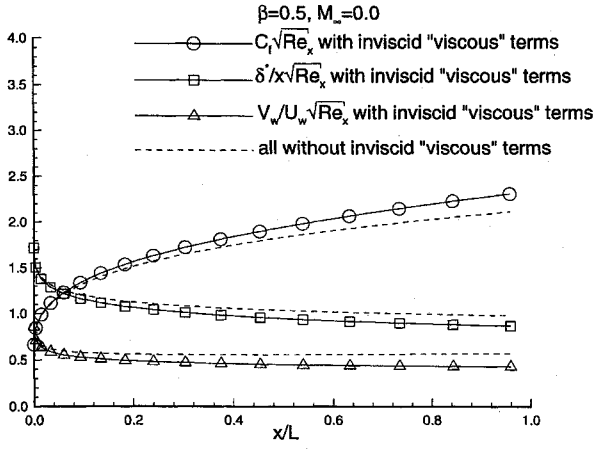

Fig. 8 Skin-friction, displacement thickness, and transpiration velocity for exponential shear flow.

boundary-layer solutions, but the second-order defect method iterated both of them.

The third case considered is inviscid shear flow given by the exponential profile

$$U/U_w = \alpha + 1 - \alpha \exp(-\beta y\sqrt{Re}/L) \tag{59}$$

Here the nondimensional results are independent of Reynolds number. Results for incompressible flow with $\alpha = 1$ and $\beta = 0.5$ are given in Figs. 7 and 8. Figure 7 gives the velocity profiles at five chordwise stations along the plate. At each station the boundary-layer solution merges with the inviscid profile smoothly. The variation of skin friction, displacement thickness, and transpiration velocity along the surface is given in Fig. 8. The skin friction increases along the plate, whereas the displacement thickness and transpiration velocity decrease. No iterations for the inviscid and boundary-layer solutions were performed.

Compressible shear flow over a flat plate was studied using the exponential inviscid profile given earlier with $\alpha = 0.1$, $M_w = 3$, and $\beta = 0.002$. Note that the inviscid temperature ratio given by Eq. (50) decreases away from the wall because the inviscid velocity increases. For $M_w = 3$, Eq. (50) gives $T_e = 0$ for $U/U_w = 1.5556$; hence, β or M_w must be small enough to keep $T_e > 0$ throughout the boundary layer. Results were calculated for a cold wall ($T_w/T_{we} = 0.1$) and a hot wall ($T_w/T_{we} = 6.0$). Figures 9 and 10 compare the velocity and temperature profiles for the cold wall case with Navier–Stokes calculations.[11] The temperature profiles exhibit the characteristic bump due to viscous dissipation. Figure 11 shows a nearly uniform distribution of skin-friction and heat transfer rate parameters along the plate. Both parameters compare within 4% of the Navier–Stokes calculations for $x/L > 0.2$. No inviscid/boundary-layer iterations were necessary because the boundary-layer displacement thickness was small due to the cold wall.

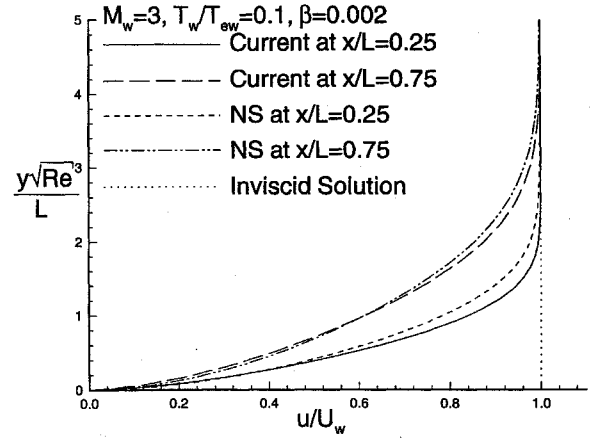

Fig. 9 Velocity profiles for cold wall.

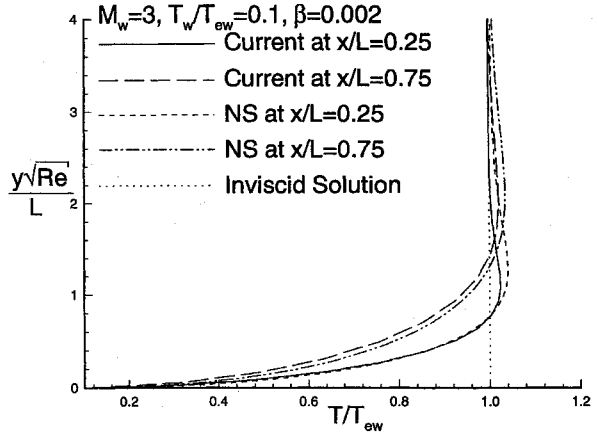

Fig. 10 Temperature profiles for cold wall.

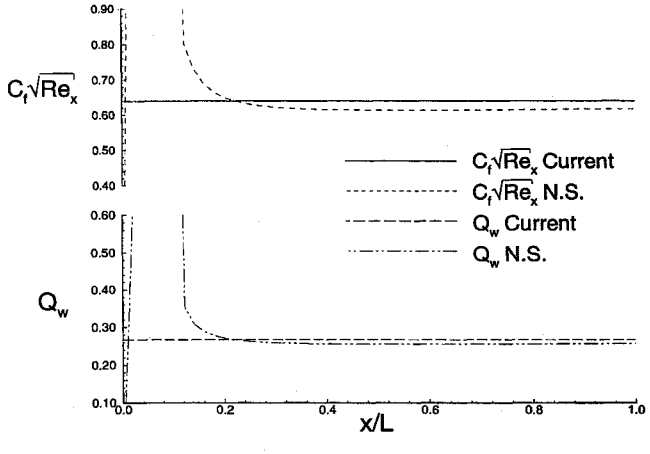

Fig. 11 Skin-friction and heat transfer for cold wall.

Figures 12 and 13 show that the velocity and temperature profiles for the hot wall case do not compare well with the Navier–Stokes calculations. In this case there is significant interaction between the boundary layer and inviscid flowfields. Figure 14 shows that a shock wave appears in the Navier–Stokes velocity profile at $x/L = 0.25$ due to the boundary-layer displacement effects. Inviscid/boundary-layer iterations would be necessary to improve the accuracy of the present method.

Numerical Accuracy

The implicit finite difference method used in this paper is second-order accurate in the normal direction and first-order accurate in the marching direction.[9] For the cases presented here $\eta_e = 8$, 40 x/L stations, $J = 41$ for the incompressible cases, and $J = 61$ for

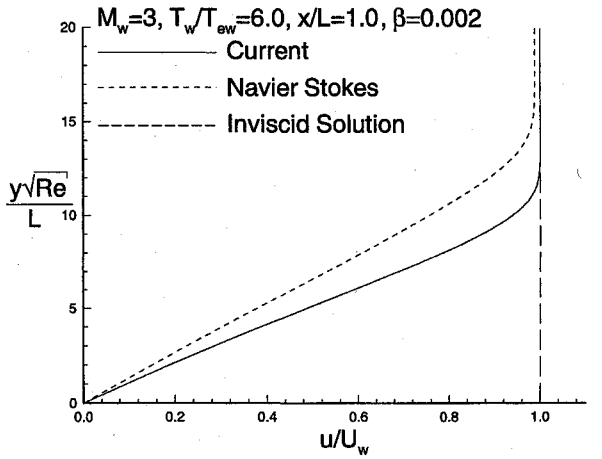

Fig. 12 Velocity profiles for hot wall.

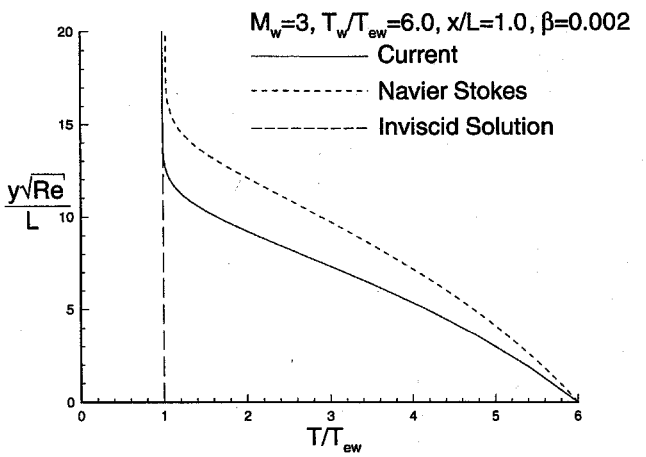

Fig. 13 Temperature profiles for hot wall.

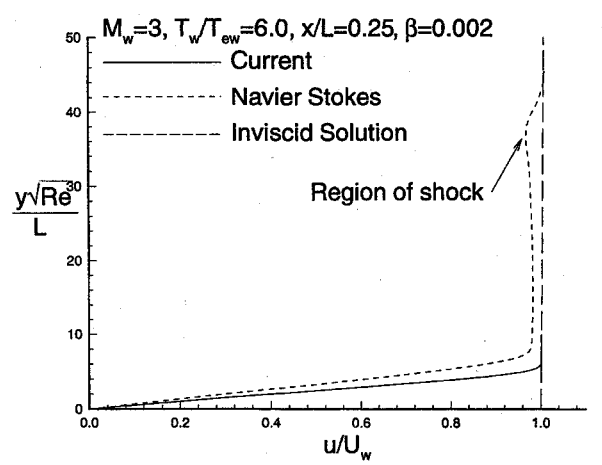

Fig. 14 Effect of shock wave on velocity profile.

the compressible cases. The accuracy of the results was tested by varying $5 < \eta_e < 10$, $20 < x/L$ stations < 80, and $21 < J < 101$. It was found that the skin-friction parameter varied less than 5% over these ranges. Increasing the x/L stations from 40 to 80 and J from 61 to 101 changed the skin-friction parameter less than 3%.

The CPU time for the Navier–Stokes calculations varied between 90 and 270 s on a Cray Y-MP, whereas the present method required less than 0.6 s on a Sun workstation for the compressible calculations. The current method has also been run on personal computers with as little as 64K RAM.

Conclusions

1. Solutions to the new boundary-layer equations will match all inviscid properties exactly with the exception of the normal velocity component.
2. The location of the outer boundary is not dependent on a boundary-layer thickness.
3. For the inviscid shear flows considered, shear has a strong effect on the skin friction for incompressible flows, but only a small effect for the compressible, cold wall case.
4. Interaction of the inviscid/boundary-layer solutions was not necessary for the incompressible and cold wall cases considered, but it is needed for the hot wall case.
5. The new boundary-layer method includes some of the inviscid/boundary-layer interaction in the first boundary-layer solution because an inviscid transpiration velocity is calculated as part of the solution.

Acknowledgments

The authors acknowledge the support of Lockheed Engineering and Science Company, Houston, TX, through LESC Subcontract 02N0166210, Stan Bouslog, technical monitor. Support was also received through NASA Cooperative Agreement NCC1-100 with the Aerothermodynamics Branch at NASA Langley Research Center, Vincent Zoby, technical monitor. The authors wish to thank Harris Hamilton, NASA Langley Research Center, for many helpful discussions, Frederick Blottner, Sandia Corporation, for providing useful references, and Jack Edwards, North Carolina State University, for providing the compressible Navier–Stokes solutions.

References

[1]Hamilton, H. H., DeJarnette, F. R., and Weilmuenster, K. J., "Application of Axisymmetric Analog for Calculating Heating in Three-Dimensional Flows," *Journal of Spacecraft and Rockets*, Vol. 24, No. 4, 1987, pp. 296–301.

[2]Zoby, E. V., Moss, J. N., and Sutton, K., "Approximate Convective-Heating Equations for Hypersonic Flows," *Journal of Spacecraft and Rockets*, Vol. 18, No. 1, 1981, pp. 64–70.

[3]Riley, C. J., and DeJarnette, F. R., "Engineering Calculations of Three-Dimensional Inviscid Hypersonic Flow Fields," *Journal of Spacecraft and Rockets*, Vol. 28, No. 6, 1991, pp. 628–635.

[4]Riley, C. J., and DeJarnette, F. R., "An Engineering Aerodynamic Heating Method for Hypersonic Flow," AIAA Paper 92-0499, Jan. 1992.

[5]Riley, C. J., "An Engineering Method for Interactive Inviscid-Boundary Layers in Three-Dimensional Hypersonic Flows," Ph.D. Dissertation, Dept. of Mechanical and Aerospace Engineering, North Carolina State Univ., Raleigh, NC, May 1992.

[6]Aupoix, B., Brazier, J. P., and Cousteix, J., "Asymptotic Defect Boundary-Layer Theory Applied to Hypersonic Flows," *AIAA Journal*, Vol. 30, No. 5, 1992, pp. 1252–1259.

[7]Monnoyer, F., Mundt, C., and Pfitzner, M., "Calculation of the Hypersonic Viscous Flow Past Reentry Vehicles with an Euler-Boundary Layer Coupling Method," AIAA 28th Aerospace Sciences Meeting, AIAA Paper 90-0417, Jan. 1990.

[8]Wuthrich, S., and Sawley, M. L., "Coupled Euler/Boundary-Layer Method for Nonequilibrium Chemically Reacting Hypersonic Flows," *AIAA Journal*, Vol. 30, No. 12, 1992, pp. 2836–2844.

[9]Blottner, F. G., "Computational Techniques for Boundary-Layers," AGARD Lecture Series No. 73, Feb. 1975.

[10]Hamilton, H. H., Millman, D. R., and Greendyke, R. B., "Finite-Difference Solution for Laminar or Turbulent Boundary Layer Flow over Axisymmetric Bodies with Ideal Gas, CF_4 or Equilibrium Air Chemistry," NASA TP 3271, Dec. 1992.

[11]Edwards, J. R., "Development of a Upwind Relaxation Multigrid Method for Computing Three-Dimensional Viscous Internal Flows," AIAA Paper 95-0208, Jan. 1995.